CONFIDENTIAL. Limited circulation. For review only.

Ensemble Kalman filtering for wind field estimation in wind farms

B. M. Doekemeijer[1], S. Boersma[1], L. Y. Pao[2] and J. W. van Wingerden[1]

Abstract— **Currently, wind farms typically rely on greedy control, in which the individual turbine's structural loading and power are optimized. However, this often appears suboptimal for the collective wind farm. A promising solution is closed-loop wind farm control using state feedback algorithms employing a dynamic model of the flow. This control method is a novelty in wind farms, and has potential to provide a temporally optimal control policy accounting for time-varying inflow conditions and unmodeled dynamics, both often neglected in current methods. An essential building block for state feedback control is a state estimator (observer) that reconstructs the system states of the dynamic model using a small number of measurements. As computational efficiency is critical in real-time control, lower-fidelity models are proposed to be used. In this work, WindFarmObserver (WFObs) is introduced, which is a state estimator relying on the WindFarmSimulator (WFSim) model and an Ensemble Kalman Filter (EnKF). The states of WFSim form the two dimensional flow field in a wind farm. In WFObs, WFSim models large scale wake dynamics, while smaller scale and stochastic effects (often neglected by current models) can be picked up by sensors and incorporated using the EnKF. WFObs is tested in a two-turbine setup using a high fidelity simulation model. With a realistic sensor setup where only** 1.1% **of the to-be-estimated states are measured, WFObs reduces the rms error by** 21% **compared to open-loop simulation, at a low computational cost of** 0.76 **s. As WFObs is sampled at** 1 **Hz, this readily allows real-time closed-loop wind farm control.**

I. INTRODUCTION

Currently, wind turbines in a wind farm are often operated following a greedy control approach. In other words, the control settings of wind turbines are optimized on an individual level for power capture and structural loads, while neglecting coupling with other turbines in the farm [1]. However, dynamic coupling between turbines is very much present due to the development of turbulent wind flow wakes. Namely, as energy is extracted from a flow by a turbine, the downstream flow has a decreased flow speed and increased turbulence intensity. In result, wind turbines experience decreased power capture and increased structural loading when operating in the wake of an upstream turbine [2]. Due to this coupling, greedy control is expected to be suboptimal to methods in which the collective power plant is considered.

Finding the collectively optimal turbine operation settings has been done in various ways. An overview of the current state of the art is given in [3]. Most often, wind farm control is done employing a simplified engineering model of the waked flow in an open-loop (feedforward) scheme (e.g., [4]–[6]). The main advantage of these models is their very low computational cost. Alternatively, control policies can be based on measurement data without employing any form of model in a closed-loop (feedback) scheme (e.g., [7]–[12]). The main advantage of this approach is that, given enough time and under constant atmospheric conditions, a (near) global optimum can be found without the need for a model.

However, most of these methods are only tested in highly idealized simulation or wind tunnel tests, and thus their applicability remains questionable. Current model-based methods typically neglect temporal and finer spatial flow dynamics by relying on a simple steady-state flow model [3]. Furthermore, model-free methods operate through online trial-and-error, but due to large-scale temporal coupling between turbines by wakes this optimization scheme is too slow for time-varying atmospheric conditions [3].

A solution to these issues is model-based closed-loop control, where both real-time measurements and an internal flow model are used in determining a control policy. While these measurements can be used to tune steady-state models, dynamic models are strongly preferred to allow the crucial inclusion of temporal wake dynamics. In this framework, measurements are used to reconstruct the system states of the dynamic model through the use of a state estimator, and this state information can then be used to find a temporally optimal control policy. This policy has potential to address changing atmospheric conditions and unmodeled (spatial and temporal) wake dynamics, both typically neglected in current methods. The main challenge in this framework is the trade-off between model accuracy and computational efficiency. As real-time control is the objective, the summed computation time of the state estimator and control law should be less than the internal sampling time of the model, which is often in the order of seconds.

The power of dynamic-model-based closed-loop control was demonstrated in [13], in which a high-fidelity model was used for predictive control under the assumption of perfect state reconstruction, showing an increase in power production of up to 16% compared to greedy control. However, iterations took $2 \cdot 10^3$ core-hours per control window, which is about seven orders of magnitude too large for real life application. This paper is therefore rather considered a benchmark tool for more time-efficient algorithms.

In the bigger picture, the authors of this paper pursue model-based closed-loop control in real time using time-efficient state estimation and control algorithms employing a medium-fidelity flow model – a novelty in wind farm control.

[1]Bart Doekemeijer, Sjoerd Boersma and Jan-Willem van Wingerden are with the Delft Center for Systems and Control (DCSC), Faculty of Mechanical Engineering, Delft University of Technology, Mekelweg 2, 2628 CD Delft, The Netherlands B.M.Doekemeijer@tudelft.nl

[2]Lucy Pao is with the Department of Electrical, Computer and Energy Engineering (ECEE), University of Colorado Boulder (CU), 1111 Engineering Dr, Boulder, 80309 CO, United States of America

Preprint submitted to 2017 American Control Conference.
Received September 19, 2016.

In this paper, a time-efficient state estimator is designed and tested that reconstructs the states of the flow model WindFarmSimulator (WFSim) [14], in which the states are the two-dimensional velocity terms and pressure terms in a farm. This state estimator, henceforth referred to as WindFarmObserver (WFObs), uses an Ensemble Kalman filter to incorporate measurements into state estimates. These state estimates can then be used in advanced control algorithms such as predictive control to calculate an optimal policy. Research on predictive control using WFSim is ongoing [15].

With respect to previous work [16], WFObs has been improved by implementing localization and inflation for accuracy (discussed in Section III-B), and parallelization for computational efficiency. Furthermore, WFObs is tested in simulation under realistic turbulence intensity, realistic measurements, and turbine yaw-misalignment.

The outline of the paper is as follows. WFSim is briefly explained in Section II. The Ensemble Kalman filter is outlined in Section III. The simulation scenario and results are discussed in Sections IV and V, respectively. We end this paper with our conclusions.

II. FLOW MODEL

In this paper, WFObs relies on a flow model on one hand, and (noisy) measurements on the other hand. WFSim developed at the Delft University of Technology is employed as the internal flow model [14]. WFSim is a medium-fidelity, dynamic flow model based on the temporally and spatially discretized two-dimensional Navier-Stokes equations. It predicts the 2D velocity vectors and pressure terms over a predefined grid in a wind farm at discrete time instants. It relies on momentum theory to model interactions between turbines and their surrounding flow. In a recent paper [14], WFSim was extended with a mixing length turbulence submodel and yaw actuation. The model boils down to solving the following set of dynamic equations

$$A\left(x_{k-1}\right)x_k = b\left(x_{k-1}, q_{k-1}\right), \tag{1}$$

for x_k at each time instant k, with $x_k = \begin{bmatrix}\overline{u}_k^T & \overline{v}_k^T & \overline{p}_k^T\end{bmatrix}^T \in \mathbb{R}^N$ the state vector containing the longitudinal velocity terms $\overline{u}_k$, lateral velocity terms $\overline{v}_k$, and pressure terms $\overline{p}_k$ in the grid at time k, and $q_k \in \mathbb{R}^M$ the system input containing the axial induction factor and yaw angle of each turbine in the wind farm.[1] Zero stress boundary conditions are incorporated. WFSim is computationally fast by exploiting sparsity in matrices $A \in \mathbb{R}^{N\times N}$ and $b \in \mathbb{R}^N$. Model validation was performed previously for a two-turbine case in a low turbulence flow with high-fidelity simulation data in [17].

Since real-time control is the objective, computational efficiency is important. As WFSim is a nonlinear model with typically $N \geq 10^3$ states, the issue of computational cost is nontrivial. This is one of the main motivations for the Ensemble Kalman filter, described next.

[1]The axial induction factor is a theoretical measure of energy extraction for a wind turbine derived from momentum theory.

III. ENSEMBLE KALMAN FILTERING

An Ensemble Kalman filter (EnKF) is employed in WFObs. The EnKF is a variant of the Kalman filter (KF) where the covariance matrices are represented by a finite sample covariance. In the literature, it has typically been applied to high-order systems derived from partial differential equations for system state reconstruction using relatively few measurements. In comparison to the regular KF, the EnKF can be applied to nonlinear systems without the need for linearization, and furthermore can be orders of magnitude faster in computation time for large systems by approximating its covariance matrices through a small number of samples [18].

A. Traditional Implementation

In this section, the key steps of the EnKF are described. Let us first define $\psi^i_{k|\ell} \in \mathbb{R}^N$ as an ensemble member with $i \in \{1,2,\ldots,N_e\} \subset \mathbb{N}$, and N_e the total number of ensemble members. Each ensemble member is a hypothesis to the true system state vector x_k with information up until time ℓ. In this paper, the measurement vector $y_\ell \in \mathbb{R}^O$, with O the number of measurements, is a subset of the state vector x_ℓ: we measure the longitudinal and lateral velocity at a small number of points in the wind field. Consequently, the mapping from x_ℓ to y_ℓ is linear and described by $y_\ell = Hx_\ell$, where $H \in \mathbb{R}^{O\times N}$ is a time-invariant matrix consisting of zeros and ones.[2]

To start the algorithm, the EnKF is initialized by distributing all N_e ensemble members around an initial state estimate $\tilde{x}_0 \in \mathbb{R}^N$, with $\tilde{x}_0^T = \begin{bmatrix}\tilde{\overline{u}}_0^T & \tilde{\overline{v}}_0^T & \tilde{\overline{p}}_0^T\end{bmatrix}$. Thus, each ensemble member $\psi^i_{0|0}$ is initialized at $\tilde{x}_0$ and summed with artificial noise $\xi^i_0 \in \mathbb{R}^N$, where ξ^i_0 has a uniform probability distribution $\mathscr{U}(-W,W)$. Entries of W can be different depending on whether they correspond to $\overline{u}$, $\overline{v}$ or $\overline{p}$.

$$\underbrace{\begin{bmatrix}\psi^1_{0|0} & \cdots & \psi^{N_e}_{0|0}\end{bmatrix}}_{\Psi_{0|0}\ \in\ \mathbb{R}^{N\times N_e}} = \begin{bmatrix}\tilde{x}_0 & \cdots & \tilde{x}_0\end{bmatrix} + \begin{bmatrix}\xi^1_0 & \cdots & \xi^{N_e}_0\end{bmatrix}. \tag{2}$$

W can be compared to the initial state error covariance matrix P_0 in the regular KF. The matrix $\Psi_{k|\ell} \in \mathbb{R}^{N\times N_e}$ is defined as the full ensemble, with column i corresponding to $\psi^i_{k|\ell}$.

Now, in the first step of each iteration, each ensemble member $\psi^i_{k-1|k-1}$ is propagated forward in time according to (1) and summed with artificial process noise $\varepsilon^i_k \in \mathbb{R}^N$, as

$$\psi^i_{k|k-1} = A(\psi^i_{k-1|k-1})^{-1} b(\psi^i_{k-1|k-1}, q_{k-1}) + \varepsilon^i_k. \tag{3}$$

In this paper, process noise $\varepsilon^i_k \in \mathbb{R}^N$ is assumed to be white noise with Gaussian distribution $\mathscr{N}(0,Q)$. Further, similar to W, Q can have different values for $\overline{u}$, $\overline{v}$ and $\overline{p}$.

In the second step, a measurement ensemble $D_k \in \mathbb{R}^{O\times N_e}$ is calculated based on the newly acquired measurements y_k summed with artificial measurement noise $\mu^i_k \in \mathbb{R}^O$.

$$D_k = \begin{bmatrix}y_k + \mu^1_k & \cdots & y_k + \mu^{N_e}_k\end{bmatrix}, \tag{4}$$

where $\mu^i_k \in \mathbb{R}^O$ is white noise with distribution $\mathscr{N}(0,R)$.

[2]While the EnKF equations presented here are for a linear state-output relationship, they can be generalized for nonlinear state-output relationships.

Preprint submitted to 2017 American Control Conference.
Received September 19, 2016.

In the third step, the ensemble members are updated using this measurement ensemble D_k. In this step, first, the deviation of each individual ensemble member to the average of all members $\Psi^{\star}_{k|k-1} \in \mathbb{R}^{N\times N_e}$ is found by

$$\Psi^{\star}_{k|k-1} = \begin{bmatrix} \psi^1_{k|k-1} & \cdots & \psi^{N_e}_{k|k-1} \end{bmatrix} \left(I_{N_e} - \frac{1}{N_e} \begin{bmatrix} 1 & \cdots & 1 \\ \vdots & \ddots & \vdots \\ 1 & \cdots & 1 \end{bmatrix} \right), \tag{5}$$

with $I_{N_e} \in \mathbb{R}^{N_e\times N_e}$ the identity matrix. Then, the analysis update of the EnKF is described by

$$\Psi_{k|k} = \Psi_{k|k-1} + (N_e-1)P^*_{k|k-1}H^T \left(\left(H\Psi^{\star}_{k|k-1}\right)\left(H\Psi^{\star}_{k|k-1}\right)^T + \begin{bmatrix} \mu^1_k & \cdots & \mu^{N_e}_k \end{bmatrix} \begin{bmatrix} (\mu^1_k)^T \\ \vdots \\ (\mu^{N_e}_k)^T \end{bmatrix} \right)^{-1} \left(D_k - H\Psi_{k|k-1}\right), \tag{6}$$

where $P^*_{k|k-1} \in \mathbb{R}^{N\times N}$ is the predicted sample-based state error covariance matrix, calculated from $\Psi^*_{k|k-1}$ as

$$P^*_{k|k-1} = \frac{1}{N_e-1}\left(\Psi^{\star}_{k|k-1}\right)\left(\Psi^{\star}_{k|k-1}\right)^T. \tag{7}$$

Since the covariance matrix is based on a finite number of ensemble members, it is a sample-based approximation of the true covariance matrix $P_{k|k-1}$ of the regular KF.

Finally, the optimal estimate $\tilde{x}_k \in \mathbb{R}^N$ of the true state vector x_k is calculated from the ensemble by taking the column-wise average of $\Psi_{k|k}$.

B. Localization and Inflation

While the EnKF has shown great potential in the literature, key issues such as inbreeding and long-range spurious correlations often spoil performance, caused by employing too small of an ensemble [19].

Inbreeding is typically defined as the situation where the error covariance matrices $P^*_{k|k-1}$ are systematically underestimated, leading to state estimates that incorrectly rely more on the internal flow model. A common method to address inbreeding is inflation, in which $P^*_{k|k-1}$ is multiplied by a constant inflation factor r at each iteration, with r typically between 1.01 and 1.20.

Long-range spurious correlations are incorrect links between measurements and states caused by sample covariances that insufficiently represent the true covariances. This leads to certain states being updated based on completely unrelated measurements. To deal with this, localization can be applied. Note that entries of $P^*_{k|k-1}$ define the correlation between two states, which in our case correspond to flow velocities or pressures at physical locations in the wind farm. This information can be used to improve the sample based estimates of the covariance matrix. The correlations with physically nearby states are increased and with far away states are decreased, thereby mitigating incorrect coupling between measurements and states. Typically, Gaspari-Cohn's fifth-order polynomial function [20] is used for localization, given by

$$\kappa(c) = \begin{cases} -\frac{1}{4}c^5 + \frac{1}{2}c^4 + \frac{5}{8}c^3 - \frac{5}{3}c^2 + 1, & \text{if } 0 \le c \le 1 \\ -\frac{1}{12}c^5 - \frac{1}{2}c^4 + \frac{5}{8}c^3 + \frac{5}{3}c^2 & \\ \qquad -5c + 4 - \frac{2}{3}\frac{1}{c}, & \text{if } 1 < c \le 2 \\ 0, & \text{otherwise} \end{cases} \tag{8}$$

in which $c = \frac{\Delta L}{z}$, with z the cut-off length after which correlation between states should be 0, and $\Delta L \ge 0$ the physical distance between two grid points. For each combination of states (8) is calculated and collected in $\overline{\kappa} \in \mathbb{R}^{N\times N}$. Localization is enforced at each iteration by taking the Hadamard product of $\overline{\kappa}$ and $P^*_{k|k-1}$.

Implementing inflation and localization in the EnKF algorithm, (7) is replaced by

$$P^*_{k|k-1} = r\cdot\overline{\kappa}\circ\left(\frac{1}{N_e-1}\left(\Psi^{\star}_{k|k-1}\right)\left(\Psi^{\star}_{k|k-1}\right)^T\right), \tag{9}$$

where $\circ$ represents the Hadamard product.

IV. SIMULATION SETUP

In Section V, the performance of WFObs will be assessed using high-fidelity simulation data. Firstly, this high-fidelity model is discussed in Section IV-A. Secondly, the wind farm topology, its spatial discretization, and the sensor (measurement) locations are described in Section IV-B. Thirdly, tuning of WFObs is described in Section IV-C.

A. Simulator for Onshore/Offshore Wind Farm Applications

To analyze the performance of WFObs, the Simulator for Onshore/Offshore Wind Farm Applications (SOWFA) [21] is employed as the "real" wind farm, from which measurements are obtained, and of which the flow fields are to be estimated. SOWFA is a software package developed by the National Renewable Energy Laboratory (NREL) that simulates flow and turbine dynamics in a wind farm at high accuracy. It relies on the three-dimensional Navier-Stokes equations, accounting for bouyancy and Coriolis effects [22]. More specifically, it employs a large-eddy simulation (LES) in which large scale dynamics are resolved directly and smaller scale dynamics are resolved using subgrid models to reduce computational cost. SOWFA is coupled with the FAST code for turbine modeling, in which rotating actuator line models are used to calculate the interactions between the turbine rotor and the flow [23]. FAST also calculates the turbine's generated power, component dynamics, and mechanical loading at multiple locations in the structure.

B. Topology, Meshing and Sensor Placement

A simulation with two NREL 5-MW turbines [24] in a turbulent atmosphere is performed in SOWFA, in which

Preprint submitted to 2017 American Control Conference.
Received September 19, 2016.

the flow is excited by yawing the upstream turbine. Three-dimensional flow fields at an increasing mesh resolution near the turbines are obtained at a sampling rate of 50 Hz. The size of grid cells varies from 3.00 m $\times$ 3.00 m $\times$ 3.02 m near the turbines, to 6.00 m $\times$ 6.00 m $\times$ 6.03 m, to 12.00 m $\times$ 12.00 m $\times$ 12.05 m on the outer parts of the domain.

At each discrete time instant of WFObs (sampled at 1 Hz), a horizontal slice at hub height is extracted from the raw SOWFA data. The data is remeshed onto the grid used in WFObs. This grid contains cells of constant size 50.65 m $\times$ 58.33 m, in a domain of 2482 m $\times$ 1400 m. The turbines are located at $(400\text{ m}, 700\text{ m})$ and $(1281.97\text{ m}, 700\text{ m})$, respectively. The grid, and WFSim boundary condition, turbine, and sensor locations for the longitudinal velocities $\overline{u}$ are displayed in Fig. 1. Those for $\overline{v}$ look very much alike, and are therefore not displayed. Pressures are not measured.

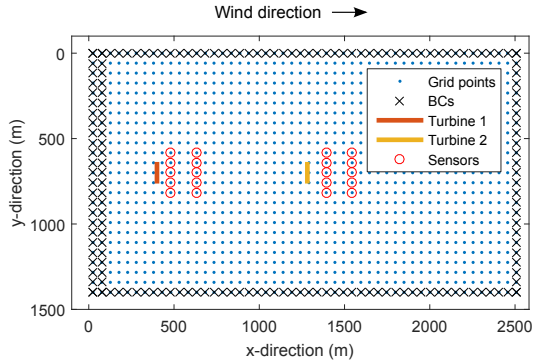

Fig. 1. Grid, and BC, turbine, and sensor locations for $\overline{u}$

Zero stress boundary conditions (BCs) are present in the north, south, and east of the grid. This meshing results in a total of $N = 3239$ states. There are a total of $O = 36$ measurements (1.1% of the states), of which 20 in $\overline{u}$ and 16 in $\overline{v}$. The same states are measured at each time instant, additionally disturbed with artificial noise with distribution $\mathcal{N}(0, 0.10)$ m/s. The number and location of measurements and the noise level are achievable with current lidar standards, a state-of-the-art technology for remote sensing [25], [26].

C. Model and Observer Tuning

Firstly, the WFSim model parameters were tuned in absence of the EnKF, as displayed in Table I. These are the free-stream flow speed u_0 and v_0, the dynamic viscosity μ_d, and air density ρ, respectively. The latter two are optimized individually according to a grid search (GS) algorithm. While a turbulence model is included in WFSim, it was not used as similar effects can be produced by manipulating μ_d. While μ_d is unrealistically high in Table I, similar trends can be noticed in the literature (e.g., [27]), and are a result of our choice to use μ_d as a tuning parameter for wake recovery, instead of using a turbulence model for this purpose.

Secondly, a sequential grid search (SGS) was performed on the EnKF in which sets of 2-4 parameters were optimized in sequence. The resulting set of optimal parameters are displayed in Table II. The order of optimization and pairs in the SGS can be seen in the third column of Table II. The SGS optimization was broken down in iterations of 3 individual optimizations of $2-4$ parameters each. Optimality is defined as the minimum averaged root-mean-square (rms) error between the true (SOWFA) and estimated (WFSim/WFObs) flow fields over a 1000 s simulation. Further, $N_e \leq 60$ was enforced to maintain low computational cost.

TABLE I
ATMOSPHERIC SETTINGS USED IN WFSIM

Variable	SOWFA	WFSim	Method
u_0	$+8.00 \pm 0.42$ m/s	8.00 m/s	Prior knowledge
v_0	-0.02 ± 0.31 m/s	0.00 m/s	Prior knowledge
μ_d	*Unknown*	$1.0 \cdot 10^2$ Pa·s	Individual GS
ρ	*Unknown*	1.2 kg·m^3	Individual GS

TABLE II
OPTIMAL PARAMETERS FOR WFOBS

Variable	WFObs	Optimized in...
Q_u	0.08 m/s	SGS step 1
Q_v	0.02 m/s	SGS step 1
R	0.10 m/s	SGS step 1
N_e	50	SGS step 2
W_u	0.90 m/s	SGS step 2
W_v	0.30 m/s	SGS step 2
r	1.025	SGS step 3
z	131 m	SGS step 3

During the SGS, it was found that Q_p and W_p can be chosen arbitrarily without affecting the quantities of interest $\overline{u}$ and $\overline{v}$, and they are therefore omitted from Table II. This is a direct consequence of the WFSim model, which calculates $\overline{p}$ as a function of $\overline{u}$ and $\overline{v}$, but not vice-versa.

V. SIMULATION RESULTS

Both WFSim (individually) and WFObs (WFSim+EnKF) are simulated for 1000 seconds with the topology and meshing according to Fig. 1, and atmospheric parameters as depicted in Table I. The flow is excited by switching the upstream turbine's yaw angle between 0° and 20° (counterclockwise in Fig. 1) following a pseudo-random binary signal. Furthermore, the parameters for the EnKF in WFObs are given in Table II. Perturbed measurements at the sensor locations from SOWFA are fed into WFObs in pursuit of improving the flow field estimations compared to using solely WFSim. The true flow fields given by SOWFA and the estimated flow fields given by WFSim and WFObs for time instants $t = 370$ s and $t = 830$ s are displayed in Fig. 2.

From the fourth and fifth column of subplots in Fig. 2, notice the significant reduction in estimation error when comparing WFSim to WFObs. The largest error arises in the wake of turbine 2, which contains complex dynamics. Further, the wake dynamics downstream of turbine 2 are strongly dependent on the operation settings of both turbines. The EnKF corrects for flow dynamics found in SOWFA which are not modeled in WFSim. Namely, WFSim overestimates the wake depth and underestimates wake recovery, which are both significantly improved in WFObs. Furthermore, the

Preprint submitted to 2017 American Control Conference.
Received September 19, 2016.

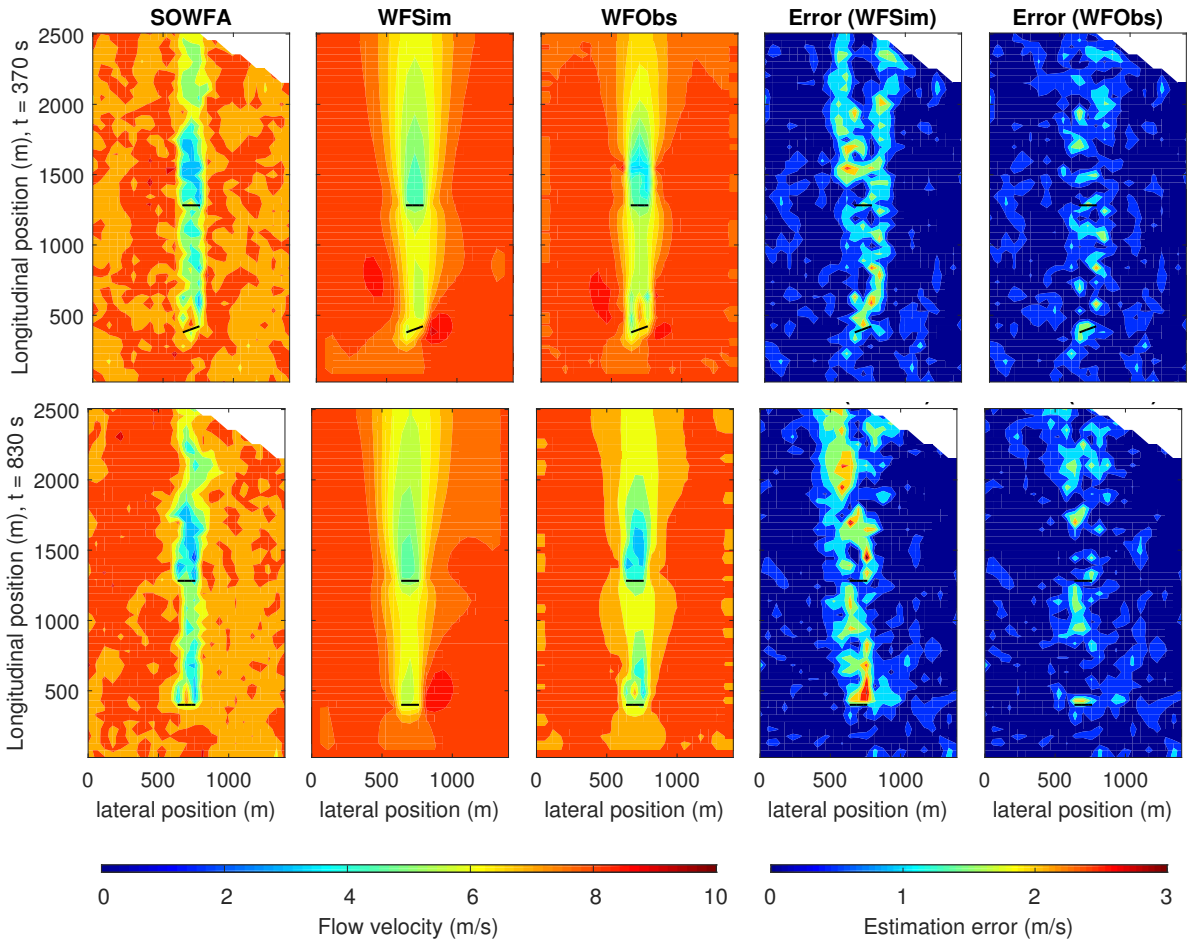

Fig. 2. Estimations of the flow field for $t = 370$ s and $t = 830$ s by WFSim and WFObs in m/s. SOWFA is assumed to be the true wind farm of which the flow properties are estimated. WFSim provides estimations solely by iterating from a set of initial conditions, while WFObs additionally takes measurements of the true flow field into account. A significant improvement is shown in WFObs, even while only 1.1% of the system outputs are available as measurements. The average root-mean-square error with SOWFA decreased from 0.638 m/s for WFSim to 0.504 m/s for WFObs. Note that a large part of the flow is uniform, which suppresses the value of quantitative improvement.

wake behind a turbine is typically not a cone-shaped structure as predicted by momentum theory, since the wake is often much weaker behind the turbine hub. This can be seen from the SOWFA data in Fig. 2, shortly downstream of turbine 1 (and somewhat behind turbine 2). The measurements allow WFObs to correct for these unmodeled flow dynamics.

Furthermore, the impact of localization and inflation as a function of the ensemble size N_e is demonstrated in Fig. 3. For these simulations, the tuning parameters did not change from Tables I and II. In Fig. 3 it is seen that incorrect coupling between measurements and states becomes increasingly present for smaller ensemble sizes, leading to poor performance. This problem is mitigated with localization. Furthermore, the performance of WFObs with localization and inflation is much more robust. For example, for $N_e = 20$ the algorithm without localization and inflation diverges, while good performance is achieved consistently if localization and inflation are applied. Actually, the EnKF requires $N_e \geq 2 \cdot 10^2$ to achieve satisfactory performance in absence of localization and inflation. Another benefit of localization is the reduction in computation time, which originates both from a reduction in the required ensemble size N_e, and a reduction in the number of floating point operations for a fixed N_e, as localization enforces a sparsification of the covariance matrices.

Finally, with computational cost being an invaluable factor in WFObs, the time per iteration comparing WFSim and WFObs is displayed in Table III.

TABLE III

COMPUTATIONAL COST PER ITERATION IN SECONDS

	N	O	N_e	time (s)
WFSim	3239	N.A.	N.A.	0.06
WFObs	3239	36	50	0.76

Note that WFObs has to evaluate (1) N_e times per iteration, yet the computational cost does not scale with N_e. This is due to parallelization in the EnKF algorithm where multiple cores are used simultaneously, as the simulation was performed on a quad-core Intel i5-4460 desktop CPU. Furthermore, the EnKF was compared to the regular KF in previous work [16], showing a reduction of computational cost by a factor of $10^2 - 10^3$, while yielding higher reconstruction accuracy. Finally, since WFObs is sampled at 1 Hz and the computational time is less than 1 s, this algorithm readily allows real-time closed-loop control.

Preprint submitted to 2017 American Control Conference.
Received September 19, 2016.

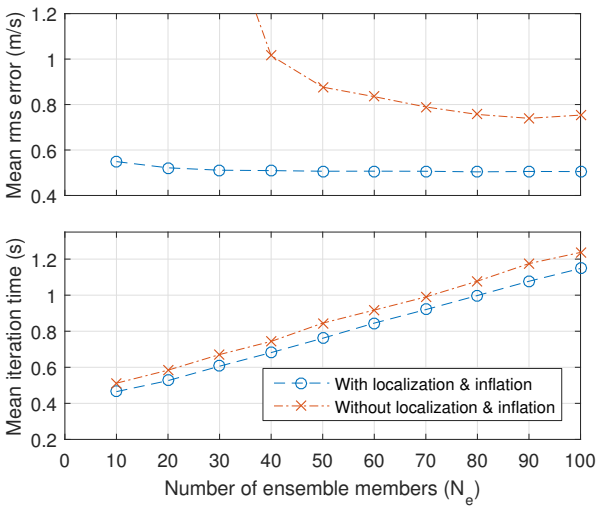

Fig. 3. Effects of localization and inflation on state estimation accuracy and computational cost. It can be seen that localization and inflation do not only significantly improve state estimation for a low number of ensemble members, they also reduce computational cost. Noticeably, for $N_e = 20$, the estimator even diverges in the absence of localization, while constant performance is achieved with localization and inflation.

VI. CONCLUSIONS

In this work, the EnKF in WFObs was extended with localization, inflation, and parallelization. furthermore, WFObs was tested at a higher level of realism using high-fidelity simulation data by incorporating turbulent flows and turbine yaw. Simulation results showed a reduction in root-mean-square error of 21% compared to open-loop simulation while requiring a low computational cost of 0.76 s. Noticeably, WFObs is able to correct for unmodeled flow dynamics such as turbine hub effects and increased wake recovery. WFObs is an essential building block and a first major step towards real-time closed-loop wind farm control using a dynamic model, which appears to be a very promising and novel concept in wind farm control.

ACKNOWLEDGMENT

We thank Matti Morzfeld, Paul Fleming and Pieter Gebraad for their invaluable contributions in this work.

REFERENCES

[1] P. Fleming, P. Gebraad, S. Lee, J.-W. van Wingerden, M. Churchfield, A. Scholbrock, J. Michalakes, K. Johnson, and P. Moriarty, "The SOWFA super-controller: A high-fidelity tool for evaluating wind plant control approaches," in *EWEA Annual Meeting*, 2013.

[2] P. Fleming, P. M. Gebraad, S. Lee, J.-W. van Wingerden, K. Johnson, M. Churchfield, J. Michalakes, P. Spalart, and P. Moriarty, "Simulation comparison of wake mitigation control strategies for a two-turbine case," *Wind Energy*, vol. 18, no. 12, pp. 2135–2143, 2015.

[3] S. Boersma, B. M. Doekemeijer, P. M. O. Gebraad, P. A. Fleming, J. Annoni, A. K. Scholbrock, and J.-W. van Wingerden, "A tutorial on control-oriented modeling and control of wind farms," in *American Control Conference*, submitted for review, May 2017.

[4] D. S. Zalkind and L. Y. Pao, "The fatigue loading effects of yaw control for wind plants," in *American Control Conference*, Jul. 2016, pp. 537–542.

[5] M. Mirzaei, T. Göçmen, G. Giebel, P. E. Sørensen, and N. K. Poulsen, "Turbine control strategies for wind farm power optimization," in *American Control Conference*, Jul. 2015, pp. 1709–1714.

[6] J. Annoni, P. M. O. Gebraad, A. K. Scholbrock, P. A. Fleming, and J.-W. van Wingerden, "Analysis of axial-induction-based wind plant control using an engineering and a high-order wind plant model," *Wind Energy*, vol. 19, no. 6, pp. 1135–1150, 2016.

[7] P. M. O. Gebraad and J.-W. van Wingerden, "Maximum power-point tracking control for wind farms," *Wind Energy*, vol. 18, no. 3, pp. 429–447, 2015.

[8] K. E. Johnson and G. Fritsch, "Assessment of extremum seeking control for wind farm energy production," *Wind Engineering*, vol. 36, no. 6, pp. 701–715, 2012.

[9] Z. Yang, Y. Li, and J. Seem, "Maximizing wind farm energy capture via nested-loop extremum seeking control," in *Dynamic Systems and Control Conference*. Oct. 2013, vol. 3.

[10] J. Park, S.-D. Kwon, and K. H. Law, "A data-driven approach for cooperative wind farm control," in *American Control Conference*, Jul. 2016, pp. 525–530.

[11] J. R. Marden, S. D. Ruben, and L. Y. Pao, "A model-free approach to wind farm control using game theoretic methods," *IEEE Transactions on Control Systems Technology*, vol. 21, no. 4, pp. 1207–1214, Jul. 2013.

[12] F. Campagnolo, A. Croce, E. M. Nanos, V. Petrović, J. Schreiber, and C. L. Bottasso, "Wind tunnel testing of a closed-loop wake deflection controller for wind farm power maximization," *Journal of Physics: Conference Series*, 2016.

[13] J. P. Goit and J. Meyers, "Optimal control of energy extraction in wind-farm boundary layers," *Journal of Fluid Mechanics*, vol. 768, 550, Feb. 2015.

[14] S. Boersma, P. M. O. Gebraad, M. Vali, B. M. Doekemeijer, and J.-W. van Wingerden, "A control-oriented dynamic wind farm flow model: WFSim," *Journal of Physics: Conference Series*, 2016.

[15] M. Vali, J.-W. van Wingerden, S. Boersma, V. Petrović, and M. Kühn, "A predictive control framework for optimal energy extraction of wind farms," *Journal of Physics: Conference Series*, 2016.

[16] B. M. Doekemeijer, J.-W. van Wingerden, S. Boersma, and L. Y. Pao, "Enhanced kalman filtering for a 2D CFD NS wind farm flow model," *Journal of Physics: Conference Series*, 2016.

[17] B. M. Doekemeijer, "Enhanced Kalman filtering for a 2D CFD Navier-Stokes wind farm model," Master's dissertation, Delft University of Technology, Jun. 2016.

[18] G. Evensen, "The Ensemble Kalman filter: Theoretical formulation and practical implementation," *Ocean Dynamics*, vol. 53, no. 4, pp. 343–367, 2003.

[19] R. E. Petrie, "Localization in the Ensemble Kalman filter," Master's dissertation, University of Reading, Aug. 2008.

[20] G. Gaspari and S. E. Cohn, "Construction of correlation functions in two and three dimensions," *Quarterly Journal of the Royal Meteorological Society*, vol. 125, no. 554, pp. 723–757, 1999.

[21] National Renewable Energy Laboratory. (Mar. 31, 2015). NWTC information portal (SOWFA), [Online]. Available: `https://nwtc.nrel.gov/SOWFA`.

[22] J. Annoni, P. Seiler, K. Johnson, P. Fleming, and P. Gebraad, "Evaluating wake models for wind farm control," in *American Control Conference*, Jun. 2014, pp. 2517–2523.

[23] P. A. Fleming, P. M. O. Gebraad, S. Lee, J.-W. van Wingerden, K. Johnson, M. Churchfield, J. Michalakes, P. Spalart, and P. Moriarty, "Evaluating techniques for redirecting turbine wakes using SOWFA," *Renewable Energy*, vol. 70, pp. 211–218, 2014.

[24] J. Jonkman, S. Butterfield, W. Musial, and G. Scott, "Definition of a 5-MW reference wind turbine for offshore system development," National Renewable Energy Laboratory (NREL), Technical report NREL/TP-500-38060, Feb. 2009.

[25] M. Courtney, R. Wagner, and P. Lindelöw, "Commercial lidar profilers for wind energy, A comparative guide," in *EWEA Annaul Meeting*, 2008.

[26] M. F. van Dooren, "Validation of the SpinnerLidar by a comparison with a sonic anemometer," University of Oldenburg, Technical report, Sep. 2016.

[27] R. N. King, P. E. Hamlington, P. Graf, and K. Dykes, "Adjoint optimization of wind farm layouts for systems engineering analysis," *AIAA-SciTech 34th Wind Energy Symposium*, Jan. 2016.